Title
Identification of Lipid Heterogeneity and Diversity in the Developing Human Brain

Journal
JACS Au, 1(12)

ISSN
2691-3704

Authors
Bhaduri, Aparna
Neumann, Elizabeth K
Kriegstein, Arnold R
et al.

Publication Date
2021-12-27

DOI
10.1021/jacsau.1c00393

Peer reviewed

JACS Au
AN OPEN ACCESS JOURNAL OF THE AMERICAN CHEMICAL SOCIETY

pubs.acs.org/jacsau

Article

Identification of Lipid Heterogeneity and Diversity in the Developing Human Brain

Aparna Bhaduri,*[,¶] Elizabeth K. Neumann,[¶] Arnold R. Kriegstein, and Jonathan V. Sweedler*

Cite This: *JACS Au* 2021, 1, 2261−2270

Read Online

ACCESS | Metrics & More | Article Recommendations | Supporting Information

ABSTRACT: The lipidome is currently understudied but fundamental to life. Within the brain, little is known about cell-type lipid heterogeneity, and even less is known about cell-to-cell lipid diversity because it is difficult to study the lipids within individual cells. Here, we used single-cell mass spectrometry-based protocols to profile the lipidomes of 154 910 single cells across ten individuals consisting of five developmental ages and five brain regions, resulting in a unique lipid atlas available via a web browser of the developing human brain. From these data, we identify differentially expressed lipids across brain structures, cortical areas, and developmental ages. We inferred lipid profiles of several major cell types from this data set and additionally detected putative cell-type specific lipids. This data set will enable further interrogation of the developing human brain lipidome.

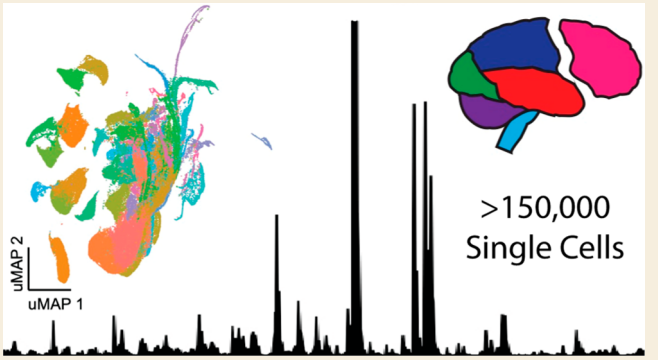

KEYWORDS: *single cell analysis, neurons, astrocytes, MALDI, mass spectrometry, development, brain*

The lipidome is a vast and understudied aspect of life. While lipids are essential to many organs, they are particularly important for brain function because they are involved in cell shape and membrane formation,[1−3] anchoring of membrane proteins,[4] and neuropeptide signaling.[5] While the lipidome is less characterized compared to other molecular classes such as proteins and genes, several efforts have served to provide key information that demonstrates the importance of lipids within neuroscience.[6−18] These studies demonstrate the importance of studying the lipidome on the single cell level within human embryonic development. Tu et al.,[18] for instance, demonstrated that glycerophospholipids decreased with age, while sphingolipids increased with age. Moreover, the human cortex is uniquely expanded compared to chimpanzees, with many of these region- and size-specific differences emerging during developmental stages.[19] This expansion also applies to the human cortical lipidome but not to other brain structures and organs.[20,21] Interestingly, the lipidome is dysregulated in the prefrontal cortex in autism,[22] suggesting a neurodevelopmental role for cortical lipid functions. However, the identification of lipid molecules in the human brain is challenging. Individual lipids are difficult to label or visualize using traditional antibody- or microscopy-based approaches, contributing to the need for alternative methods to access and survey their content.

RESULTS

To study the lipidome of the developing human brain, we created an experimental and analytical approach that enables large-scale single-cell lipidomic data set generation. While this study focuses upon the developing human cortex, the methods employed here address the data scale and analysis time required for atlas- or repository-type studies, which are of current interest to the NIH and other funding agencies (HuBMAP,[23] HCA,[24] HTAN,[25] and the BRAIN Initiative[26]), though optimization in an individual system is advisible, especially if working with a hard to dissociate tissue. We began by dissecting primary post-mortem early and midgestation tissue samples into known anatomical brain regions. Cell dissociates were collected from ten individuals across five brain regions at early developmental stages, and across cortical regions for later time points (Figure S1A; Table S1). Samples were dissociated and plated with glycerol onto indium tin-oxide coated slides. Single-cell matrix-assisted laser desorption/ionization (MALDI) mass spectrometry (MS) analysis was performed as previously described.[27,28] Data were normalized to the total ion current and aligned with in-house scripts (see

Received: September 6, 2021
Published: November 11, 2021

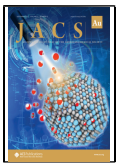

https://doi.org/10.1021/jacsau.1c00393
JACS Au 2021, 1, 2261−2270

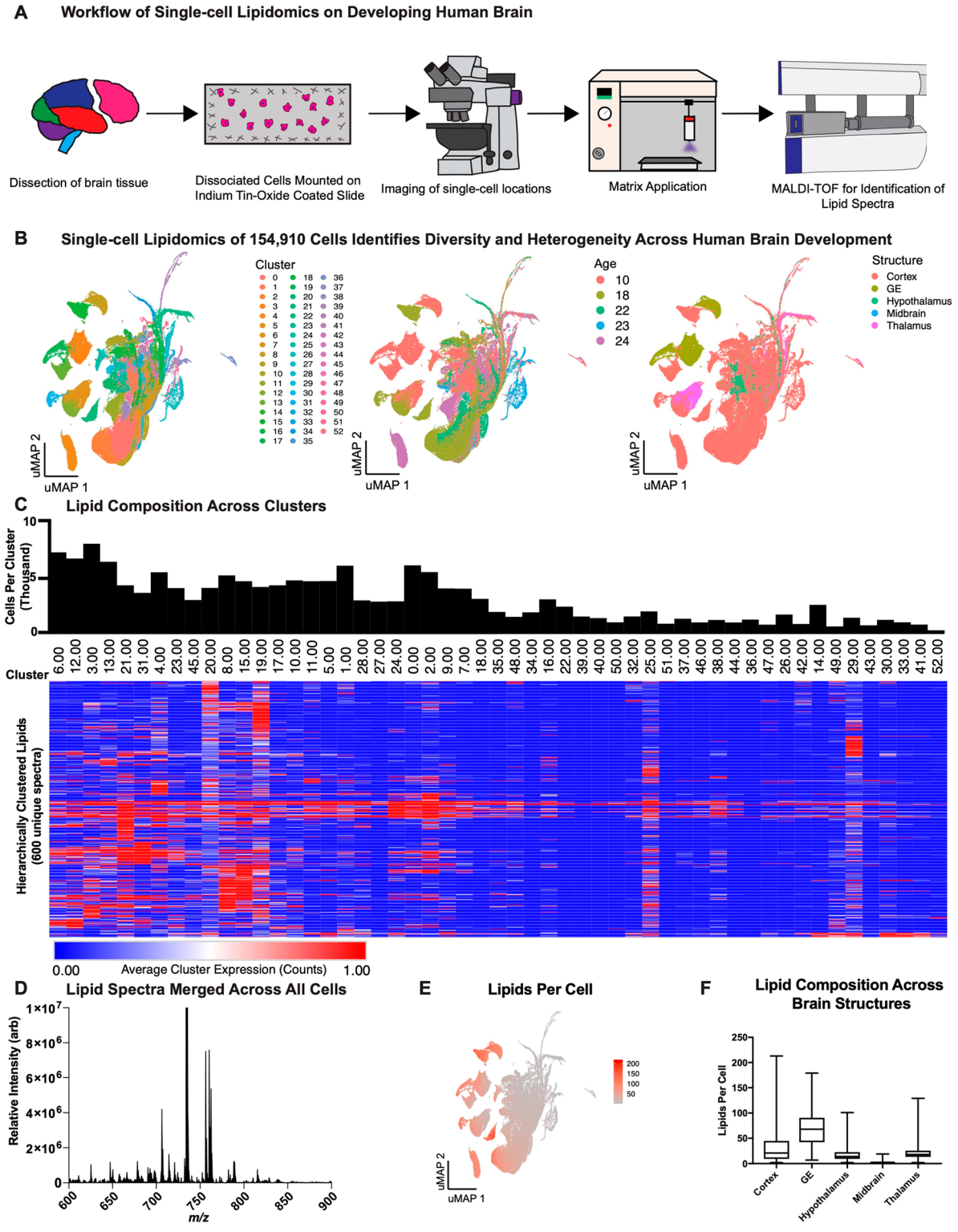

Figure 1. Single-cell mass spectrometry identifies lipid diversity in the developing human brain. (A) Single-cell lipidomics was performed on the cortex, ganglionic eminences (GE), hypothalamus, midbrain, and thalamus of the developing human brain between gestational weeks (GW) 10–23. In brief, brain regions were dissected and dissociated into single cells. These slides were then processed using MALDI-TOF to identify lipid spectra for 154 910 cells. (B) Fifty-three unique lipidomic clusters (left) visualized by uniform manifold approximation and projection (UMAP) were identified via Louvain clustering. Some of these clusters were enriched by specific ages in gestational weeks that were sampled (middle) or brain structures (right), while other clusters were intermixed across stages or regions. (C) Hierarchical clustering shows the average abundance of each detected lipid within a cluster. On average, there were 2923 cells per cluster ranging from 184 to 9153. (D) Summed mass spectra from all cells, demonstrating how bulk analysis is insufficient for assaying lipid diversity. (E) The UMAP recolored by number of cells. (F) The distribution of lipids per cell for each sampled brain structure.

https://doi.org/10.1021/jacsau.1c00393
JACS Au 2021, 1, 2261–2270

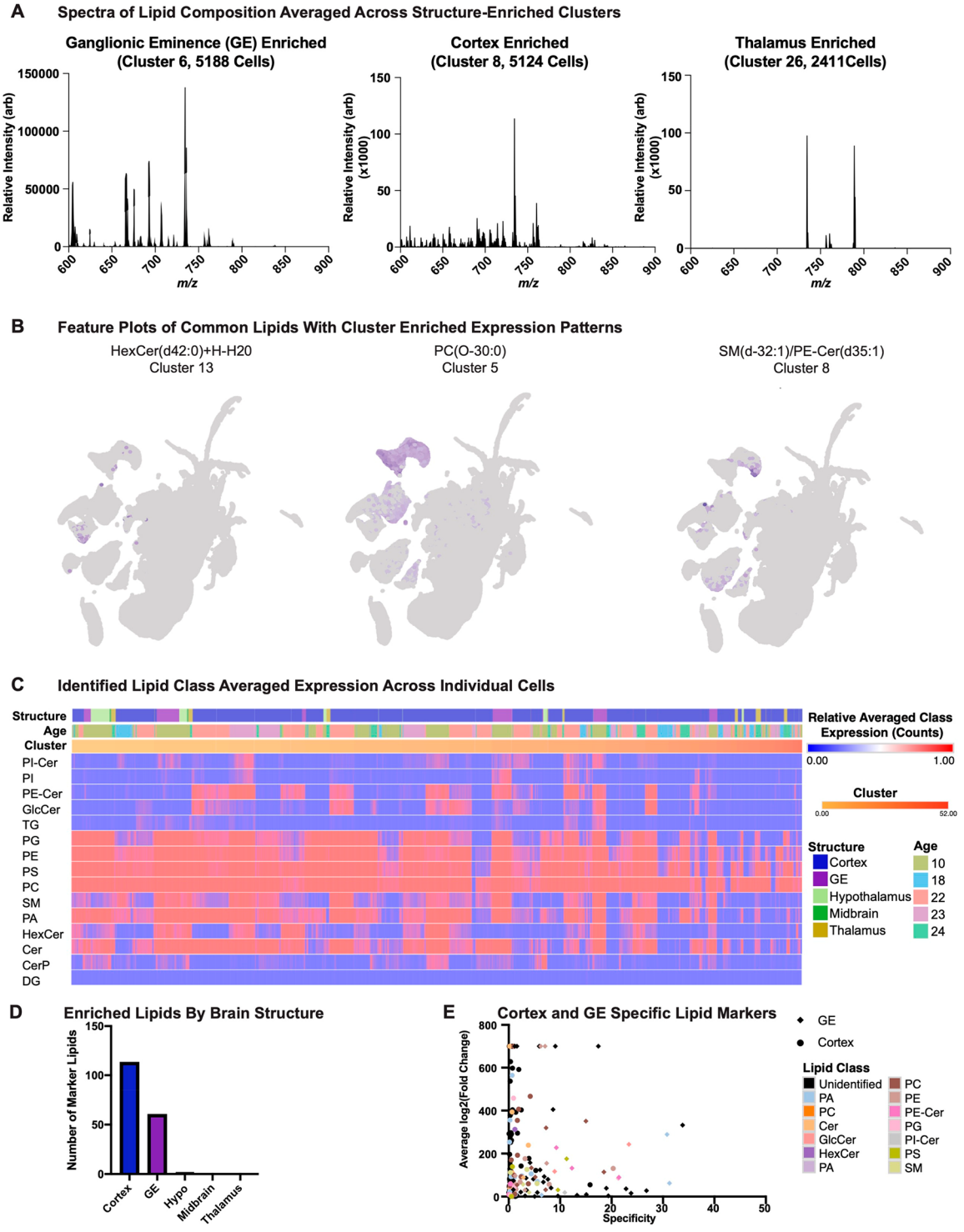

Figure 2. Lipid heterogeneity in the developing human brain. (A) Averaged lipid spectra from 3 clusters, where clusters 6, 8, and 26, are GE, cortex, and thalamus enriched, respectively, highlight that there many different lipids detected in the brain and there are unique lipid combinations across brain structures. (B) Three commonly detected lipids with cluster level enrichments as feature plots in the UMAP space, with more purple signal indicating greater detection of that lipid in a cell. (C) The hierarchically clustered (using rows) heat map shows each cell in the data set in the columns with summed signal across each lipid class, with a high abundance of PC and PE coverage, as expected. (PI-Cer: phosphoinositol ceramide; PI: phosphoinositol; PE-Cer: phosphoethanolamine ceramide; GlcCer: glucosylceramide; TG: triglyceride; PG: phosphoglyceride; PE: phosphoethanolamine; PS: phosphotidylserine; PC: phosphatidylcholine; SM: sphingomyelin; PA: phosphatidic acid; HexCer: hexosylceramide; Cer: ceramide; GalCer: galactosylceramide; CerP: ceramide phosphate; DG: diglyceride) (D) Differential expression analysis was performed across all cells based upon their brain structure. The number of lipid markers per structure is depicted here. Full list of differential lipids is presented in Table S6. (E) For the cortex and GE lipid markers, they are plotted based upon their average fold change and specificity (calculated as percent of cells in the structures in which the lipid was detected divided by percent of cells in all other structures in which the lipid was detected). Points are colored by lipid class, if the lipid was identified, otherwise the point is black. Cortex lipids are indicated by a circular point, GE by a diamond point.

https://doi.org/10.1021/jacsau.1c00393
JACS Au 2021, 1, 2261−2270

Methods). We obtained a total of 154 910 single-cell lipidomic profiles. Lipid identities were assigned based on a combination of mass accuracy, orthogonal Fourier transform ion cyclotron resonance (FT-ICR) MS measurements, and LIPIDMAPS database search.[29,30] The listed lipids included common salt adducts which are present in the sample, such as sodium, or added as a during sample preparation, such as formate. Additionally, the extent of lipid saturation was also not considered, except when assessing which lipid identity was more likely. While there is significant functional relevance within neuronal axons, the lipids measured here within the soma represent biological relevance associated with cell shape, protein anchoring, and developmental processes prior to extensive morphological maturation.[31,32]

One challenge of MS analysis across primary tissue samples, time points, and time scales is the increased potential for nonbiological (e.g., instrumental and sampling) variance. We examined the replicability in our data and observed an average Pearson's correlation between individuals and brain structures of 0.41 and 0.48, respectively, with samples from the same brain region and age corresponding with a correlation of greater than 0.6 (Figure S1B; Table S2), which is similar to parallel, early single-cell transcriptomic studies.[33] These analyses highlight that although there is some variability across lipidomic profiles which is to be expected given that lipidomes are unlikely to remain stable through various physiological inputs, there are enough similarities observed with this method to characterize the scope of single-cell lipid diversity and heterogeneity. While the measurements acquired here took place over the course of a year because of sample acquisition and instrument time, we have previously demonstrated reproducibility[34] and here demonstrate the variance is not a result of analysis date or time (Figure S1). Moreover, the replicability suggests that aspects of the lipidome are widely expressed and reproducibly generated during development.

We performed clustering analysis to group the cells based on similar lipid content. Overall, the data was best described by 53 clusters, some of which were enriched for specific brain structures or developmental stages (Figure 1B; Figure S1C, D). We observed that the lipid content across clusters was diverse, with 600 lipids being represented in unique combinations and abundances when averaged across individual cluster groups (Figure 1C; Tables S3 and S4). On average, we detected 35 different lipids within a cell, with a range of 2−213 lipids per cell, though the distribution was similar across developmental ages (Figure 1D, E; Figure S1E). Of note, the number of detected lipids per cell varied with brain structures such that the cortex and ganglionic eminences (GE) had the highest number of distinct lipids detected per cell (Figure 1F). Previous work noted highlighted higher concentrations of lipids in adult gray matter and other brain structures, such as the medulla, but these concentration measurements are agnostic to lipid diversity.[35,36]

It is important to highlight that there are potential confounding variables such as age and anatomical area, which may explain our observations. For example, it may be that some brain structures have complex distributed lipid content where most individual lipids are below our instrumental detection limit so that those cells appear less diverse. Interestingly, low lipid numbers per cell (<10) corresponded to cells sampled from younger, noncortical regions while cells with high lipid numbers (>150) were more correlated with cells samples from older, cortical regions.

To investigate the biological underpinnings of our data and how specific lipids may correspond to cell type or biological function, we putatively identified 287 of the 600 lipids in our data set (Table S5) using a combination of LIPIDMAPS, and orthogonal FT-ICR MS measurements.[37−39] While the assignments here were made with high mass accuracy measurements, there are isomeric lipid species that we cannot differentiate with this method. It is difficult to perform tandem MS on even the highest abundance species at cellular resolution and cannot fragment species that are only present in a few cells. We used the assignment we believe to be the most likely; we acknowledge these are not confirmed, nor are we considering isomers which will be a future endeavor of the field, such as through the inclusion of ion mobility spectrometry. We extracted lipid profiles from clusters enriched for different brain structures. We observed that [phosphatidylcholine (PC) (32:0)+H]$^+$ is most often the base peak of each spectrum (Figure 2A, Figures S2 and S3). We highlighted common brain lipids that had specific cluster expression (Figure 2B) and determined age-, region-, and cluster-specific lipid class expression patterns (Figure 2C). Across all cells, we found some lipids that were detected within most clusters (PC(32,0) in all 53 clusters) but many lipids were only localized in a handful of clusters (e.g., HexCer(d42:0) + H − H_2O, PC(O-30:0), and PS(O-20:0)) (Figure S4). This highlights that although the time points explored in this study precede myelination and other large-scale lipid production events, lipids may play key functional roles in regulating cell type-specific functions at specific developmental time points. For instance, clusters 4, 11, and 24 are partially defined by the presence of plasmalogens (Table S4), known to be accumulated during development,[40−42] and their dysregulation leads to neurological diseases,[42,43] implicating their importance. Despite these findings, the role of specific plasmalogens is not known. Here, we have determined the abundance of specific lipids within these clusters, such as PA(O-36:2), PA(O-34:0), and PC(O-28:0) defining cluster 4 (Table S4). Through these types of analyses and future experiments, we can potentially begin to parse out which specific lipids may be responsible for essential developmental functions.

We sought to utilize the analysis of different brain structures as a way to identify classes of lipids with regional specificity. In a heat map of all lipid classes hierarchically clustered across all cells, we noted that triglycerides (TG) were enriched in the ganglionic eminences (GE) (Figure 2C), which give rise to the vast majority of inhibitory interneurons during human cortical development,[44] suggesting triglycerides may in promote the generation and/or migration of these cell populations. To further explore structural enrichments, we used differential expression analysis across all cells based upon their dissected brain structure. Concordant with the lower detected lipid content per cell in the hypothalamus, midbrain, and thalamus, we observed few lipids enriched as markers in these structures (Figure 2D, Table S6). Thus, we focused more deeply on the cortex and GE, two telencephalic structures that are developmentally related but diverge at later time points; the cortex expands during development and gives rise to the six neuronal layers and many glial populations,[45] while the GE is a transitional structure that disappears before birth.[46] The lipid classes were approximately equally represented within the cortex and GE (Table S6), but discrete lipid profiles were different. For example, individual phosphatidic acid (PA) and ceramides (Cer) were both more specific and abundant in the

https://doi.org/10.1021/jacsau.1c00393
JACS Au 2021, 1, 2261−2270

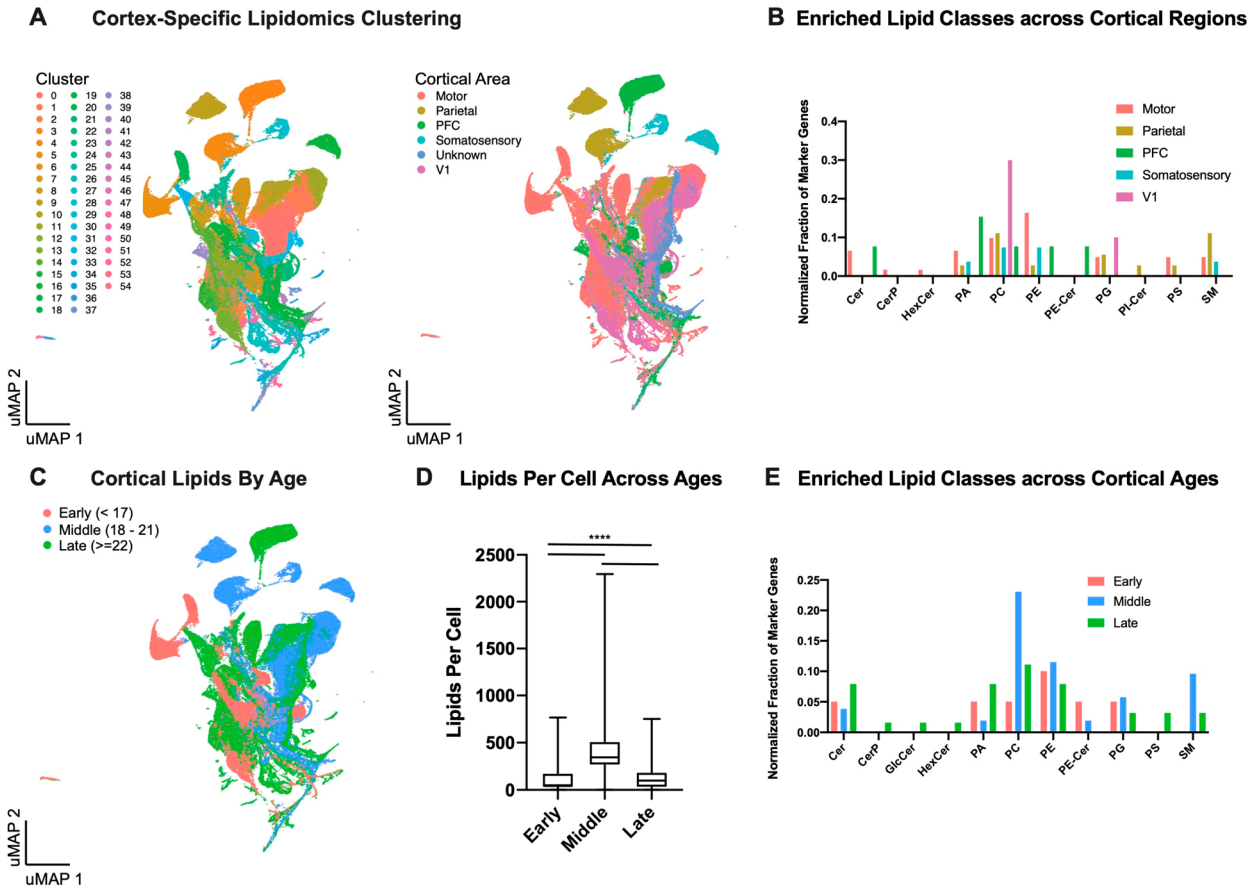

Figure 3. Cortex lipidome analysis. (A) Single-cell lipidomics was used as the input for cell clustering of the cells derived from the cortex alone, resulting in 55 clusters (left) and included some cortical area-specific clusters (middle). (B) Lipid markers were calculated across cortical regions. The number of identified lipids in each class were counted, and normalized by dividing by the total number of marker lipids for that area, creating the plotted normalized fraction of marker genes. Each represented lipid class is shown in groups on the *x*-axis, with bars colored by the cortical area being represented. (C) The UMAP plot of the cortex analysis is colored by the age of the samples, shown in the legend by GW. (D) Box and whisker plots show the number of lipids per cell for each age range in the cortex data. (E) Lipid markers were calculated across cortical stages of development. The number of identified lipids in each class were counted, and normalized by dividing by the total number of marker lipids for that area, creating the plotted normalized fraction of marker genes. Each represented lipid class is shown in groups on the *x*-axis, with bars colored by the cortical age range being represented.

GE, whereas lipids specific to the cortex had lower levels of enrichment (Figure 2E). Here, we defined specificity as the relative enrichment of a lipid in a cluster compared to the rest of the clusters, and we do observe some examples of large fold changes with lower specificity in cases of highly variable lipid representation across cells.

We also performed the same clustering analysis on the cortical cells alone (Figure 3A, Tables S7 and S8). Recent work has shown that across cortical regions, excitatory neurons are transcriptionally distinct and these differences emerge during developmental time points.[47] Interestingly, because many genes that distinguishing these cortical regions revolve around lipid metabolism, we sought to explore how these regions are distinct in terms of their lipid composition. We again performed differential expression analysis, but this time across cortical regions (Table S8). Using these markers, we investigated what proportion of lipid area markers were from each of the identified lipid classes (Figure 3B). Strikingly, we see a strong distinction between frontal areas (PFC, motor, somatosensory) and occipital areas, mirroring known gradients and transcriptional programs.[48] For example, ceramides (Cer, HexCer, PE-Cer, PI-Cer) are enriched in frontal cortical regions and help regulate signaling cascades.[47] By contrast, phosphatidylcholines (PC) are comparatively enriched in V1 dissected regions, suggesting that membrane composition is not constant across cortical regions, and may play a role in cortical arealization.

We further explored the cortex across developmental time points, binning the ages sampled into early (before GW17, before peak-neurogenesis), middle (GW18−21, during peak neurogenesis), and late (GW22 − GW24, after peak neurogenesis and at the beginning of gliogenesis)[49] (Figure 3C). In the cortex alone, we observed a significant increase in the number of identifiable lipids that during stages of peak neurogenesis (Figure 3D). Differential lipid analysis was performed across these age ranges (Table S9), and we noted an enrichment of PC during the middle developmental stages, with late stages only having lipid enrichments of phosphatidylserine (PS), and other ceramide classes including HexCer, CerP, and GlcCer (Figure 3E). Notably, PS double in content and are involved in metabolism of acetylcholine and other transmitters.[50] Enrichment of PC lipids in the middle ages is reminiscent of the V1 PC enrichment across areas and may be indicative of a maturation difference, as V1 neuronal differentiation lags behind frontal areas.

https://doi.org/10.1021/jacsau.1c00393
JACS Au 2021, 1, 2261−2270

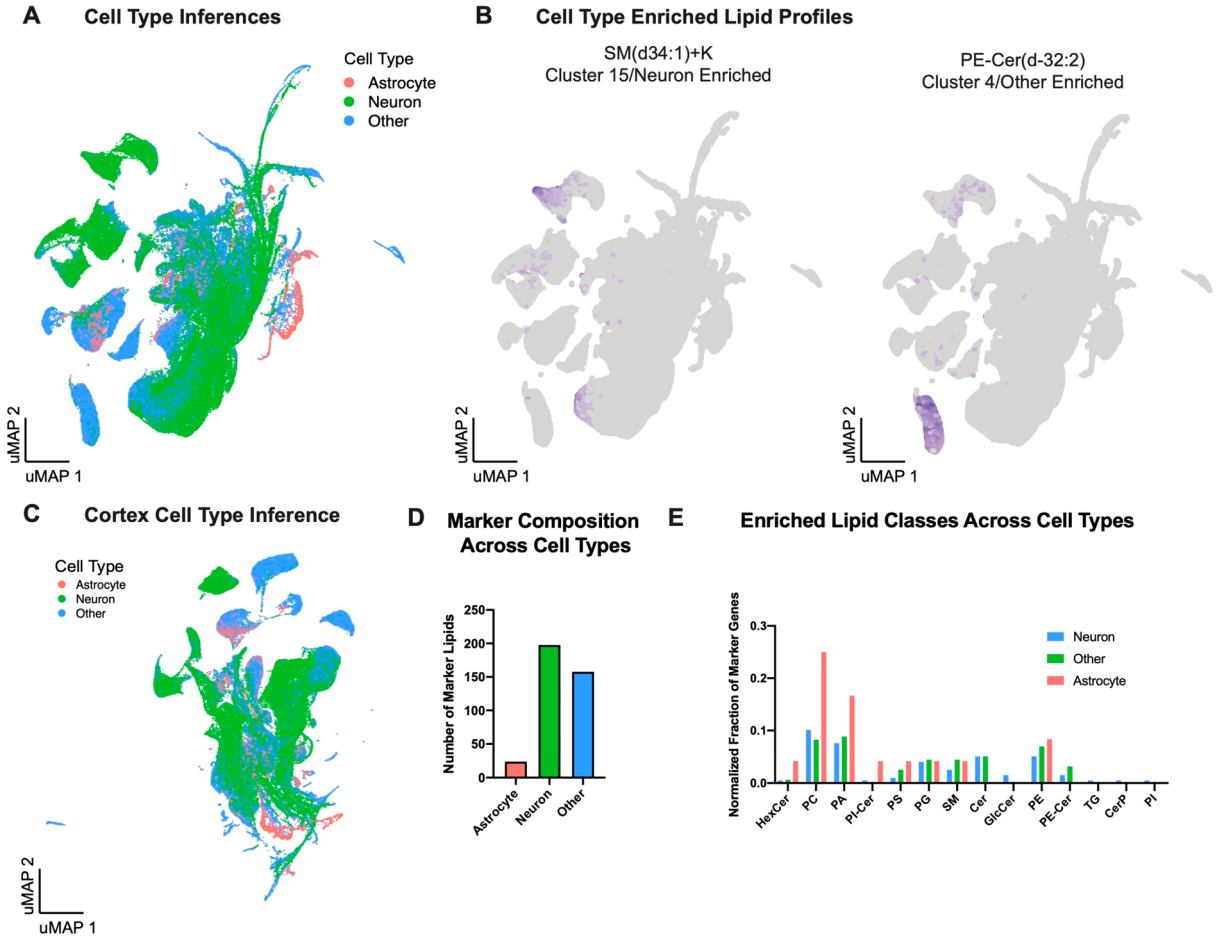

Figure 4. Lipid-based classification of cell class. (A) Using known cell-type specific lipids, we classified each cell in our data as either neuron, astrocyte, or other, as shown in the recolored UMAP diagram. (B) Feature plots of two lipids that are strongly cluster and cell type enriched suggest that lipids may have strong cell type correspondence. (C) Cortical cells could also be presumptively assigned a cell class, and we observe some cell class and cortical area specific cluster assignments (right). (E) Lipid markers were calculated across inferred cell types. The number of identified lipids in each class were counted, and normalized by dividing by the total number of marker lipids for that area, creating the plotted normalized fraction of marker genes. Each represented lipid class is shown in groups on the *x*-axis, with bars colored by the cell type being represented.

To explore potential cell type-specific lipid composition, we used 16 lipids that are known to differentiate enriched neurons and astrocytes.[28,51−54] This annotation enabled putative assignments neurons, astrocytes (which may include radial glia progenitors), and other cell types (likely including vasculature and microglia) (Figure 4A, B). We established that 25 clusters consist of mostly neurons, 20 clusters are associated with glia, and 8 clusters are comprised of other cell types. Cells with small numbers of detected lipids (<10) were more likely to be categorized as from neuronal or glial populations, whereas cells with large numbers of detected lipids were enriched for "other" cell types. We then used differential expression across these putative groups and expanded the lipids associated with these classes to include SM(d-30:0), SM(d42:1), and Cer(d44:1) for neurons, and PA(O-34:0), PG(O-34:0), and PC(O-28:0) for astrocytes (Table S10), among others. In total, we correlated an additional 149 lipids to neurons and 14 to astrocytes across all brain structures. The diversity observed in neurons is not surprising, because of the drastic changes that neurons undergo during development.[55]

This analysis enabled us to identify an additional 200 lipids that differentiate glial populations and neurons within the cortex (Figure 4C, Table S10). In particular, we found 10 lipids that defined astrocytes within the cortical regions and 104 lipids that defined neurons (Figure 4D, E). We identified numerous area-specific and cell-type enriched lipids, including groups of ceramides and phosphatidylcholines that show unique expression in one cortical area (Figure S5A), consistent with the areal analysis presented earlier. Similar unique classes are identifiable in the cortex, GE, and hypothalamus at early stages of brain development (Figure S5B). These data suggest that the transcriptomic differences across brain and cortical regions (Table S11) manifest lipid composition differences as well. Across cell types, there were many more lipid markers of neuronal and other cell populations than for astrocytes, possibly because astrocytes emerge at later time points and have less complex lipid composition. Overall, astrocytes had stronger relative representation of HexCer, PC, and PA lipid markers, cellular populations excluding neurons and glia were defined by TG, CerP, and PI lipid classes. This observation is consistent with a recent analysis of mouse astrocyte lipids.[56] More work is required to characterize what, if any, functional roles are played by these specific lipids or lipid classes across brain regions or cortical structures, or if these unique profiles can be directly linked to area-specific transcriptional profiles that have been previously identified.[47]

https://doi.org/10.1021/jacsau.1c00393
JACS Au 2021, 1, 2261−2270

DISCUSSION

Here, we provide previously unreported detail of the lipid diversity and heterogeneity that exists during human brain development. Because of the inherent limitations surrounding many approaches used to assess lipid content at the single-cell level, this analytical process enables the exploration of these lipids.

While the work here represents over a hundred thousand cells, we recognize that we are profiling the highest abundance molecular species within the individual cells, and it is likely that each individual cell contains more than 213 lipids (the maximum number we identified in a single cell); we cannot characterize lipids present in amounts below the detection limit of our instrumentation. Additionally, there were many ions that could not be assigned and this could be a result of being associated with lipid classes not comprehensively included in LIPIDMAPS, nonlipid molecular features, or uncharacterized species. From this data set, we identify lipid composition patterns that describe brain regionalization, cortical arealization, changes across developmental stages in the cortex, and characterize broad cell type identities. Future work will be required to build upon this descriptive data set to explore the functional role of various lipid classes and their impact upon cell-fate specification and other core biological processes in human brain development. Current open questions that exist based upon this data resource include whether or not lipids are "passive" readouts of other cellular processes, or act as regulators of cell fate specification. This is especially pertinent within radial glia and neural progenitor populations. These single-cell lipidome characterizations across developmental time points of the human cortex and other brain regions are the first step toward understanding how lipid composition changes as a function of development. One of the most challenging aspects of analyzing biological samples is that they exist within the tissue matrix in a wide range of concentrations that surpasses the dynamic range of a mass spectrometer (and most other instrumental approaches). While methods exist for reducing this complexity, such as integrating a separation prior to the measurement, they reduce the total number of cells that can be analyzed, particularly at true cellular resolution. As such, many of the lipids detected are at higher concentrations within the analyzed cell. In some cases, using single cell methods, we can detect less common lipids that are at locally higher concentrations in specific cells but present at lower overall concentrations within the whole tissue. Finally, we also acknowledge that the dissociation procedure may both affect the proportion of cell types that remain viable as well as affect highly reactive lipid species. These effects will be the focus of future experiments, but do not diminish the utility of the hypothesis generating data set depicted here

Intriguingly, in the data we present here, we observe a diversity and heterogeneity of lipids prior to the onset of synaptogenesis[56] and most cell−cell communication that comprise many of the known functional role of lipids in brain biology. For example, we see an increase in the number of lipids per cell during peak neurogenesis, with many unique clusters and lipid profiles spanning cortical regions. Is this volume and diversity of lipid content a function of rapid division and migration, or do lipids offer relevant cues during this dynamic period of development? We also observe enrichment of ceramides in various regions and time points. As these are precursors to sphingolipids, they may be indicators of increasing cell type and functional complexity within the developing human brain, and have also been described as regulators of differentiation and stem cell proliferation.[57,58] One limitation to further understanding these relationships is the incomplete mapping of lipids to transcriptomic and proteomic readouts of cell identity. Improved understanding of which enzymes, transporters, and interaction partners impact lipid composition in a cell may help us more easily interpret the observations from this lipid atlas, including through direct connections between transcriptomic cell types and lipid clusters as it is currently unclear if they correlate with transcriptomic definitions or offer orthogonal markers of identity. The cell types presented in this manuscript are an approximation based upon enriched neuronal and glial populations. More specific subtyping of cell types/states would improve the relevance of these data sets, especially given the degree to which transcriptomic diversity of cell types in the developing human brain have been described in other studies. Currently the technology to perform the joint profiling required to make these correspondences is not yet available, but our findings of distinct lipidomic profiles in progenitor and neuronal populations should further motivate the development of these types of multiomic approaches. Moreover, as technological advances improve sensitivity, more lipids may be detectable in individual cells, allowing us an even fuller picture of the lipid profiles during human brain development.

To make this data useful to the broader community, we developed a lipid browser to explore these data. From this browser (https://cells.ucsc.edu/?ds=brain-lipids) (Figure S6), individuals can observe the UMAPs we present in this study and color them by metadata properties, download the entire data set, explore lipid cluster markers, and browse m/z spectra. In making this data accessible, we hope that the community will continue to dissect and build upon a new frontier of single-cell biology to better contextualize the role that lipids play in developmental processes.

METHODS

Chemicals

2,5-Dihydroxybenzoic acid (DHB) and ethanol were purchased from MilliporeSigma (St. Louis, MO). Hoechst 33342 was purchased from Life Technologies (Gaithersburg, MD). Peptide Calibration Standard Kit II (angiotensin II, angiotensin I, substance P, bombesin, ACTH clip 1−17, ACTH clip 18−39, somatostatin 28, bradykinin fragment 1−7) was purchased from Bruker Corp. (Billerica, MA). All reagents were used as received (>98% purity) without further purification.

Sample Collection

Samples were obtained from developing human brain tissue donated through the San Francisco General Hospital. All samples used in this study were collected with informed consent and collection was approved by the UCSF Human Gamete, Embryo and Stem Cell Research Committee (GESCR) protocol 10−03379. To our knowledge, all samples were developmentally and chromosomally normal. After sample collection, samples were processed within 2 h; during the intervening transportation and transfer time, samples were kept on ice and in artificial cerebral spinal fluid (ACSF: 125 mM NaCl, 2.5 mM KCl, 1 mM $MgCl_2$, 1 mM $CaCl_2$, 1.25 mM NaH_2PO_4, 25 mm $NaHCO_3$, 25 mm D-glucose, bubbled with 95% O_2 and 5% CO_2) to maintain the health of the cells. Brain regions were dissected and samples dissociated into single-cell mixtures using papain (Worthington, NJ). Previous work with a live/dead stain showed us that papain results in high levels of viability after creating a single-cell suspension.[47] All samples were processed in the same way, and

https://doi.org/10.1021/jacsau.1c00393
JACS Au 2021, 1, 2261−2270

dissociated cells were viable, as verified by a trypan blue live/dead cell count. These cells were resuspended in equal volumes of PBS with 0.04% PFA and 80% glycerol in PBS and dropped onto the slide. Single-cell mixtures were counted, and 400 000 cells were mounted onto each indium−tin oxide coated glass slide (Delta Technologies, Loveland, CO), marked by hand-etched fiduciary marks in the shape of crosses. The slides were left at room temperature overnight and excess glycerol was gently tipped off.

Optical Imaging

Brightfield and fluorescence images were acquired on a Zeiss Axio M2 microscope (Carl Zeiss Microscopy GmbH, Oberkochen, Germany) equipped with an Ab cam Icc5 camera, X-cite Series 120 Q mercury lamp (Lumen Dynamics, Mississauga, Canada), and a HAL 100 halogen illuminator (Carl Zeiss Microscopy GmbH). The DAPI (ex. 335−383 nm; em. 420−470 nm) dichroic filter was used for fluorescence excitation. The images were acquired with a 10× objective (1 pixel-width is 0.55 μm) with a 13% overlap produced during image tiling. Images were processed and exported as big tiff files using ZEN software, version 2, blue edition (Carl Zeiss Microscopy GmbH).

MS Analysis

microMS was used as previously described to obtain coordinates of individual cells.[59] Briefly, cells were filtered by size (>8 μm in diameter), shape and distance (the cells must be located at least 100 μm distance from each other). These criteria reduce the time spent analyzing debris and artifacts from cell sampling; this approach was used to register microscopy images with the MALDI MS stage by locating stage coordinates for at least 15 fiduciary points present on the slide. After full-slide imaging was performed, slides were coated with a 50 mg/mL DHB solution dissolved in 1:1 ethanol:water with 0.1% trifluoroacetic acid as described previously using a custom automated sprayer.[28] The matrix solution was nebulized at 10 mL/h using nitrogen gas at 50 psi with 100 passes. Samples were taped to a rotating plate and the spray was placed 3 cm above the samples. The total amount of matrix applied was between 0.1 and 0.2 mg/cm2. Single-cell analysis was performed on an ultrafleXtreme TOF/TOF mass spectrometer (Bruker Corp.) with the reflectron activated and a mass window of 500−3000. The "Ultra" (~100 μm footprint) laser setting was used and 300 laser shots were accumulated at 1000 Hz and 60% laser energy for each cell. The instrument was calibrated with a quadratic fit using the standard Bruker peptide mix. Lipid extracts of select samples were prepared using the Bligh−Dyer method59. Direct infusion electrospray ionization of lipid extract (~1 mg of dried extract was resuspended in 1 mL of 50:50 methanol and water) was performed for high mass accuracy of selected lipids using a solariX XR 7T Fourier-transform ion cyclotron resonance (FTICR) mass spectrometer (Bruker Corp.) with a mass window of m/z 100−3000 yielding a transient length of 1.96 s in positive ion mode. Sample was delivered at 120 μL/h with a capillary voltage of 3900 V. Additional instrumental parameters include: broadband detection, 0.100 s ion accumulation, 0.001 s time-of-flight, 4.0 L/min dry gas flow, capillary exit of 220 V, deflector plate at 200 V, skimmer 1 at 15 V, octopole RF amplitude of 350 Vpp, a quadrupole mass cut off of 150 m/z, collision cell entrance voltage of −1.5 V, 1 ICR fill, a front and back trap plate of 1.5 V, and an excitation power of 7.1 dB. Extract spectra were recalibrated using $[PC(32:0)+H]^+$, $[PC(32:0)+Na]^+$, $[PC(38,4)+H]^+$.

Data Normalization and Lipid Identification

Spectra were normalized to the total ion current and aligned using $[PC(32:0)+H]^+$, which was present in most of the single cells. Lipids were putatively identified using a combination of high mass accuracy FT-ICR MS and LIPIDMAPS database searching [10.1021/ed200088u, 10.1093/nar/gkm324] using >3 ppm errors as a cut off. The m/z values obtained from the ultrafleXtreme were mass matched to the closest identity obtained using the FT-ICR spectra. Upon analysis in Seurat, we also regressed out batch in the space of normalized values in order to ensure comparison across samples with potential batch effects.

Clustering

Clustering was performed using Louvain−Jaccard graph-based clustering. Normalized matrices were used for downstream analysis without additional transformation. Variable genes were identified based upon default parameters in Seurat version 2. In the space of these variable genes, principal component analysis was performed, and significant principal components were identified based upon previously described methods60. The 10 nearest neighbors of each individual cell were identified based upon the projection of these principal components with the RANN R package (CRAN), and the Jaccard distance was calculated between all nearest neighbors, expanding distance between only slightly similar cells and decreasing the distances between similar cells. Clusters were determined with the igraph R package (https://igraph.org/) using Louvain clustering, and differential spectra were identified using the Wilcoxon rank sum test.

Cell Type Annotation

Cell type annotations were used by comparing identifiable lipids between each individual cell in our data set and previously published[28] cell-type-specific lipid profiles [PE(O-34:2)/PE(P-34:1), PE(38:2), PE(O-36:2)/PE(P-36:1), PC(O-34:1)/PC(P-34:0), SM-(d36:1), PC(32:1), PC(40:6), PC(34:0), PC(38:6), PC(32:0)/PE(35:0), PC(36:2), PC(34,1), PE(36,4), PC(34,0), PC(O-36:2)/PC(P-36:1)]. If more than 70% of the annotated lipids matched, it was assigned as either astrocyte or neuron, but if the match for either cell type was less than this, it was labeled as other.

■ ASSOCIATED CONTENT

Supporting Information

The Supporting Information is available free of charge at https://pubs.acs.org/doi/10.1021/jacsau.1c00393.

Supporting figures S1−S6 and associated legends (PDF)

Tables, including metadata, annotations, and lipid identifications (XLXS)

■ AUTHOR INFORMATION

Corresponding Authors

Aparna Bhaduri − *Department of Neurology, University of California, San Francisco, San Francisco, California 94143, United States; The Eli and Edythe Broad Center of Regeneration Medicine and Stem Cell Research, University of California, San Francisco, San Francisco, California 94143, United States; Department of Biological Chemistry, University of California, Los Angeles, Los Angeles, California 90095, United States;* orcid.org/0000-0003-4625-6899; Email: ABhaduri@mednet.ucla.edu

Jonathan V. Sweedler − *Department of Chemistry, Beckman Institute for Advanced Science and Technology, and Neuroscience Program, University of Illinois at Urbana−Champaign, Urbana, Illinois 61801, United States;* orcid.org/0000-0003-3107-9922; Email: jsweedle@illinois.edu

Authors

Elizabeth K. Neumann − *Department of Chemistry and Beckman Institute for Advanced Science and Technology, University of Illinois at Urbana−Champaign, Urbana, Illinois 61801, United States;* orcid.org/0000-0002-6078-3321

Arnold R. Kriegstein − *Department of Neurology, University of California, San Francisco, San Francisco, California 94143, United States; The Eli and Edythe Broad Center of Regeneration Medicine and Stem Cell Research, University of*

https://doi.org/10.1021/jacsau.1c00393
JACS Au 2021, 1, 2261−2270

California, San Francisco, San Francisco, California 94143, United States

Complete contact information is available at: https://pubs.acs.org/10.1021/jacsau.1c00393

Author Contributions

[¶]A.B. and E.K.N. contributed equally.

Notes

The authors declare no competing financial interest.

■ ACKNOWLEDGMENTS

We thank Beatriz Alvarado and Diane Jung for technical assistance. The authors acknowledge support from the National Institute of Neurological Disorders and Stroke Award No. K99 NS111731, a L'Oreal/AAAS For Women In Science Fellowship (to A.B.), the National Institute of Mental Health Award No. 1U01MH109062 (to J.V.S.) and the National Institute on Drug Abuse Award No. P30DA018310 (to J.V.S.). E.K.N. acknowledges support from the National Science Foundation Graduate Research Fellowship Program and a Springborn Fellowship. The data for this study is available in a processed, browsable, and downloadable format at https://cells.ucsc.edu/?bp=brain&ds=brain-lipids. In addition, raw data will be submitted to the Illinois Data Bank (https://databank.illinois.edu/) and is currently available upon request.

■ REFERENCES

(1) Janmey, P. A.; Kinnunen, P. K. Biophysical properties of lipids and dynamic membranes. *Trends Cell Biol.* **2006**, *16* (10), 538−46.

(2) Simons, K.; Vaz, W. L. Model systems, lipid rafts, and cell membranes. *Annu. Rev. Biophys. Biomol. Struct.* **2004**, *33*, 269−95.

(3) van Meer, G.; Voelker, D. R.; Feigenson, G. W. Membrane lipids: where they are and how they behave. *Nat. Rev. Mol. Cell Biol.* **2008**, *9* (2), 112−24.

(4) Marsh, D.; Horvath, L. I.; Swamy, M. J.; Mantripragada, S.; Kleinschmidt, J. H. Interaction of membrane-spanning proteins with peripheral and lipid-anchored membrane proteins: perspectives from protein-lipid interactions (Review). *Mol. Membr. Biol.* **2002**, *19* (4), 247−55.

(5) Tracey, T. J.; Steyn, F. J.; Wolvetang, E. J.; Ngo, S. T. Neuronal Lipid Metabolism: Multiple Pathways Driving Functional Outcomes in Health and Disease. *Front. Mol. Neurosci.* **2018**, *11*, 10.

(6) Naudi, A.; Cabre, R.; Jove, M.; Ayala, V.; Gonzalo, H.; Portero-Otin, M.; Ferrer, I.; Pamplona, R. Lipidomics of human brain aging and Alzheimer's disease pathology. *Int. Rev. Neurobiol.* **2015**, *122*, 133−89.

(7) Piomelli, D.; Astarita, G.; Rapaka, R. A neuroscientist's guide to lipidomics. *Nat. Rev. Neurosci.* **2007**, *8* (10), 743−54.

(8) Wang, C.; Palavicini, J. P.; Han, X. Lipidomics Profiling of Myelin. *Methods Mol. Biol.* **2018**, *1791*, 37−50.

(9) Enriquez-Algeciras, M.; Bhattacharya, S. K. Lipidomic mass spectrometry and its application in neuroscience. *World J. Biol. Chem.* **2013**, *4* (4), 102−10.

(10) Ji, J.; Kline, A. E.; Amoscato, A.; Samhan-Arias, A. K.; Sparvero, L. J.; Tyurin, V. A.; Tyurina, Y. Y.; Fink, B.; Manole, M. D.; Puccio, A. M.; Okonkwo, D. O.; Cheng, J. P.; Alexander, H.; Clark, R. S.; Kochanek, P. M.; Wipf, P.; Kagan, V. E.; Bayir, H. Lipidomics identifies cardiolipin oxidation as a mitochondrial target for redox therapy of brain injury. *Nat. Neurosci.* **2012**, *15* (10), 1407−13.

(11) Merrill, C. B.; Basit, A.; Armirotti, A.; Jia, Y.; Gall, C. M.; Lynch, G.; Piomelli, D. Patch clamp-assisted single neuron lipidomics. *Sci. Rep.* **2017**, *7* (1), 5318.

(12) Blasco, H.; Veyrat-Durebex, C.; Bocca, C.; Patin, F.; Vourc'h, P.; Kouassi Nzoughet, J.; Lenaers, G.; Andres, C. R.; Simard, G.; Corcia, P.; Reynier, P. Lipidomics Reveals Cerebrospinal-Fluid Signatures of ALS. *Sci. Rep.* **2017**, *7* (1), 17652.

(13) Pousinis, P.; Ramos, I. R.; Woodroofe, M. N.; Cole, L. M. Lipidomic UPLC-MS/MS Profiles of Normal-Appearing White Matter Differentiate Primary and Secondary Progressive Multiple Sclerosis. *Metabolites* **2020**, *10* (9), 366.

(14) Walther, A.; Cannistraci, C. V.; Simons, K.; Duran, C.; Gerl, M. J.; Wehrli, S.; Kirschbaum, C. Lipidomics in Major Depressive Disorder. *Front Psychiatry* **2018**, *9*, 459.

(15) Wood, P. L. Lipidomics of Alzheimer's disease: current status. *Alzheimer's Res. Ther.* **2012**, *4* (1), 5.

(16) Astarita, G.; Stocchero, M.; Paglia, G. Unbiased Lipidomics and Metabolomics of Human Brain Samples. *Methods Mol. Biol.* **2018**, *1750*, 255−269.

(17) Kim, W. S.; Jary, E.; Pickford, R.; He, Y.; Ahmed, R. M.; Piguet, O.; Hodges, J. R.; Halliday, G. M. Lipidomics Analysis of Behavioral Variant Frontotemporal Dementia: A Scope for Biomarker Development. *Front Neurol* **2018**, *9*, 104.

(18) Tu, J.; Yin, Y.; Xu, M.; Wang, R.; Zhu, Z. J. Absolute quantitative lipidomics reveals lipidome-wide alterations in aging brain. *Metabolomics* **2018**, *14* (1), 5.

(19) Sakai, T.; Hirata, S.; Fuwa, K.; Sugama, K.; Kusunoki, K.; Makishima, H.; Eguchi, T.; Yamada, S.; Ogihara, N.; Takeshita, H. Fetal brain development in chimpanzees versus humans. *Curr. Biol.* **2012**, *22* (18), R791−2.

(20) Li, Q.; Bozek, K.; Xu, C.; Guo, Y.; Sun, J.; Paabo, S.; Sherwood, C. C.; Hof, P. R.; Ely, J. J.; Li, Y.; Willmitzer, L.; Giavalisco, P.; Khaitovich, P. Changes in Lipidome Composition during Brain Development in Humans, Chimpanzees, and Macaque Monkeys. *Mol. Biol. Evol.* **2017**, *34* (5), 1155−1166.

(21) Bozek, K.; Wei, Y.; Yan, Z.; Liu, X.; Xiong, J.; Sugimoto, M.; Tomita, M.; Paabo, S.; Sherwood, C. C.; Hof, P. R.; Ely, J. J.; Li, Y.; Steinhauser, D.; Willmitzer, L.; Giavalisco, P.; Khaitovich, P. Organization and evolution of brain lipidome revealed by large-scale analysis of human, chimpanzee, macaque, and mouse tissues. *Neuron* **2015**, *85* (4), 695−702.

(22) Yu, Q.; He, Z.; Zubkov, D.; Huang, S.; Kurochkin, I.; Yang, X.; Halene, T.; Willmitzer, L.; Giavalisco, P.; Akbarian, S.; Khaitovich, P. Lipidome alterations in human prefrontal cortex during development, aging, and cognitive disorders. *Mol. Psychiatry* **2020**, *25*, 2952.

(23) Hu, B. C. The human body at cellular resolution: the NIH Human Biomolecular Atlas Program. *Nature* **2019**, *574* (7777), 187−192.

(24) Regev, A.; Teichmann, S. A.; Lander, E. S.; Amit, I.; Benoist, C.; Birney, E.; Bodenmiller, B.; Campbell, P.; Carninci, P.; Clatworthy, M.; Clevers, H.; Deplancke, B.; Dunham, I.; Eberwine, J.; Eils, R.; Enard, W.; Farmer, A.; Fugger, L.; Gottgens, B.; Hacohen, N.; Haniffa, M.; Hemberg, M.; Kim, S.; Klenerman, P.; Kriegstein, A.; Lein, E.; Linnarsson, S.; Lundberg, E.; Lundeberg, J.; Majumder, P.; Marioni, J. C.; Merad, M.; Mhlanga, M.; Nawijn, M.; Netea, M.; Nolan, G.; Pe'er, D.; Phillipakis, A.; Ponting, C. P.; Quake, S.; Reik, W.; Rozenblatt-Rosen, O.; Sanes, J.; Satija, R.; Schumacher, T. N.; Shalek, A.; Shapiro, E.; Sharma, P.; Shin, J. W.; Stegle, O.; Stratton, M.; Stubbington, M. J. T.; Theis, F. J.; Uhlen, M.; van Oudenaarden, A.; Wagner, A.; Watt, F.; Weissman, J.; Wold, B.; Xavier, R.; Yosef, N.; Human Cell Atlas Meeting, P., The Human Cell Atlas. *eLife* **2017**, *6* DOI: 10.7554/eLife.27041.

(25) Rozenblatt-Rosen, O.; Regev, A.; Oberdoerffer, P.; Nawy, T.; Hupalowska, A.; Rood, J. E.; Ashenberg, O.; Cerami, E.; Coffey, R. J.; Demir, E.; Ding, L.; Esplin, E. D.; Ford, J. M.; Goecks, J.; Ghosh, S.; Gray, J. W.; Guinney, J.; Hanlon, S. E.; Hughes, S. K.; Hwang, E. S.; Iacobuzio-Donahue, C. A.; Jane-Valbuena, J.; Johnson, B. E.; Lau, K. S.; Lively, T.; Mazzilli, S. A.; Pe'er, D.; Santagata, S.; Shalek, A. K.; Schapiro, D.; Snyder, M. P.; Sorger, P. K.; Spira, A. E.; Srivastava, S.; Tan, K.; West, R. B.; Williams, E. H.; Human Tumor Atlas, N. The Human Tumor Atlas Network: Charting Tumor Transitions across Space and Time at Single-Cell Resolution. *Cell* **2020**, *181* (2), 236−249.

(26) Ecker, J. R.; Geschwind, D. H.; Kriegstein, A. R.; Ngai, J.; Osten, P.; Polioudakis, D.; Regev, A.; Sestan, N.; Wickersham, I. R.; Zeng, H. The BRAIN Initiative Cell Census Consortium: Lessons Learned toward Generating a Comprehensive Brain Cell Atlas. *Neuron* **2017**, *96* (3), 542−557.
(27) Neumann, E. K.; Ellis, J. F.; Triplett, A. E.; Rubakhin, S. S.; Sweedler, J. V. Lipid Analysis of 30000 Individual Rodent Cerebellar Cells Using High-Resolution Mass Spectrometry. *Anal. Chem.* **2019**, *91* (12), 7871−7878.
(28) Neumann, E. K.; Comi, T. J.; Rubakhin, S. S.; Sweedler, J. V. Lipid Heterogeneity between Astrocytes and Neurons Revealed by Single-Cell MALDI-MS Combined with Immunocytochemical Classification. *Angew. Chem., Int. Ed.* **2019**, *58* (18), 5910−5914.
(29) Fahy, E.; Sud, M.; Cotter, D.; Subramaniam, S. LIPID MAPS online tools for lipid research. *Nucleic acids research* **2007**, *35*, W606−12.
(30) Fahy, E.; Subramaniam, S.; Murphy, R. C.; Nishijima, M.; Raetz, C. R.; Shimizu, T.; Spener, F.; van Meer, G.; Wakelam, M. J.; Dennis, E. A. Update of the LIPID MAPS comprehensive classification system for lipids. *J. Lipid Res.* **2009**, *50* (Suppl), S9−14.
(31) Barabas, M. E.; Mattson, E. C.; Aboualizadeh, E.; Hirschmugl, C. J.; Stucky, C. L. Chemical structure and morphology of dorsal root ganglion neurons from naive and inflamed mice. *J. Biol. Chem.* **2014**, *289* (49), 34241−9.
(32) Safinya, C. R.; Raviv, U.; Needleman, D. J.; Zidovska, A.; Choi, M. C.; Ojeda-Lopez, M. A.; Ewert, K. K.; Li, Y.; Miller, H. P.; Quispe, J.; Carragher, B.; Potter, C. S.; Kim, M. W.; Feinstein, S. C.; Wilson, L. Nanoscale assembly in biological systems: from neuronal cytoskeletal proteins to curvature stabilizing lipids. *Adv. Mater.* **2011**, *23* (20), 2260−70.
(33) Ramskold, D.; Luo, S.; Wang, Y. C.; Li, R.; Deng, Q.; Faridani, O. R.; Daniels, G. A.; Khrebtukova, I.; Loring, J. F.; Laurent, L. C.; Schroth, G. P.; Sandberg, R. Full-length mRNA-Seq from single-cell levels of RNA and individual circulating tumor cells. *Nat. Biotechnol.* **2012**, *30* (8), 777−82.
(34) Xie, Y. R.; Castro, D. C.; Bell, S. E.; Rubakhin, S. S.; Sweedler, J. V. Single-Cell Classification Using Mass Spectrometry through Interpretable Machine Learning. *Anal. Chem.* **2020**, *92* (13), 9338−9347.
(35) O'Brien, J. S.; Sampson, E. L. Lipid composition of the normal human brain: gray matter, white matter, and myelin. *J. Lipid Res.* **1965**, *6* (4), 537−44.
(36) Chavko, M.; Nemoto, E. M.; Melick, J. A. Regional lipid composition in the rat brain. *Mol. Chem. Neuropathol.* **1993**, *18* (1−2), 123−31.
(37) Abbott, S. K.; Jenner, A. M.; Mitchell, T. W.; Brown, S. H.; Halliday, G. M.; Garner, B. An improved high-throughput lipid extraction method for the analysis of human brain lipids. *Lipids* **2013**, *48* (3), 307−18.
(38) Baba, T.; Campbell, J. L.; Le Blanc, J. C. Y.; Baker, P. R. S.; Ikeda, K. Quantitative structural multiclass lipidomics using differential mobility: electron impact excitation of ions from organics (EIEIO) mass spectrometry. *J. Lipid Res.* **2018**, *59* (5), 910−919.
(39) Chan, R. B.; Oliveira, T. G.; Cortes, E. P.; Honig, L. S.; Duff, K. E.; Small, S. A.; Wenk, M. R.; Shui, G.; Di Paolo, G. Comparative lipidomic analysis of mouse and human brain with Alzheimer disease. *J. Biol. Chem.* **2012**, *287* (4), 2678−88.
(40) Tulodziecka, K.; Diaz-Rohrer, B. B.; Farley, M. M.; Chan, R. B.; Di Paolo, G.; Levental, K. R.; Waxham, M. N.; Levental, I. Remodeling of the postsynaptic plasma membrane during neural development. *Mol. Biol. Cell* **2016**, *27* (22), 3480−3489.
(41) Horibata, Y.; Elpeleg, O.; Eran, A.; Hirabayashi, Y.; Savitzki, D.; Tal, G.; Mandel, H.; Sugimoto, H. EPT1 (selenoprotein I) is critical for the neural development and maintenance of plasmalogen in humans. *J. Lipid Res.* **2018**, *59* (6), 1015−1026.
(42) Dorninger, F.; Herbst, R.; Kravic, B.; Camurdanoglu, B. Z.; Macinkovic, I.; Zeitler, G.; Forss-Petter, S.; Strack, S.; Khan, M. M.; Waterham, H. R.; Rudolf, R.; Hashemolhosseini, S.; Berger, J. Reduced muscle strength in ether lipid-deficient mice is accompanied by altered development and function of the neuromuscular junction. *J. Neurochem.* **2017**, *143* (5), 569−583.
(43) Paul, S.; Lancaster, G. I.; Meikle, P. J. Plasmalogens: A potential therapeutic target for neurodegenerative and cardiometabolic disease. *Prog. Lipid Res.* **2019**, *74*, 186−195.
(44) Wamsley, B.; Fishell, G. Genetic and activity-dependent mechanisms underlying interneuron diversity. *Nat. Rev. Neurosci.* **2017**, *18* (5), 299−309.
(45) Rakic, P. The radial edifice of cortical architecture: from neuronal silhouettes to genetic engineering. *Brain Res. Rev.* **2007**, *55* (2), 204−19.
(46) Encha-Razavi, F.; Sonigo, P. Features of the developing brain. *Childs Nerv Syst* **2003**, *19* (7−8), 426−8.
(47) Nowakowski, T. J.; Bhaduri, A.; Pollen, A. A.; Alvarado, B.; Mostajo-Radji, M. A.; Di Lullo, E.; Haeussler, M.; Sandoval-Espinosa, C.; Liu, S. J.; Velmeshev, D.; Ounadjela, J. R.; Shuga, J.; Wang, X.; Lim, D. A.; West, J. A.; Leyrat, A. A.; Kent, W. J.; Kriegstein, A. R. Spatiotemporal gene expression trajectories reveal developmental hierarchies of the human cortex. *Science* **2017**, *358* (6368), 1318−1323.
(48) Cadwell, C. R.; Bhaduri, A.; Mostajo-Radji, M. A.; Keefe, M. G.; Nowakowski, T. J. Development and Arealization of the Cerebral Cortex. *Neuron* **2019**, *103* (6), 980−1004.
(49) Lui, J. H.; Hansen, D. V.; Kriegstein, A. R. Development and evolution of the human neocortex. *Cell* **2011**, *146* (1), 18−36.
(50) Glade, M. J.; Smith, K. Phosphatidylserine and the human brain. *Nutrition* **2015**, *31* (6), 781−6.
(51) Gonzalez de San Roman, E.; Bidmon, H. J.; Malisic, M.; Susnea, I.; Kuppers, A.; Hubbers, R.; Wree, A.; Nischwitz, V.; Amunts, K.; Huesgen, P. F. Molecular composition of the human primary visual cortex profiled by multimodal mass spectrometry imaging. *Brain Struct. Funct.* **2018**, *223* (6), 2767−2783.
(52) Sugiura, Y.; Konishi, Y.; Zaima, N.; Kajihara, S.; Nakanishi, H.; Taguchi, R.; Setou, M. Visualization of the cell-selective distribution of PUFA-containing phosphatidylcholines in mouse brain by imaging mass spectrometry. *J. Lipid Res.* **2009**, *50* (9), 1776−88.
(53) Sugiyama, E.; Yao, I.; Setou, M. Visualization of local phosphatidylcholine synthesis within hippocampal neurons using a compartmentalized culture system and imaging mass spectrometry. *Biochem. Biophys. Res. Commun.* **2018**, *495* (1), 1048−1054.
(54) Yang, H.-J.; Sugiura, Y.; Ishizaki, I.; Sanada, N.; Ikegami, K.; Zaima, N.; Shrivas, K.; Setou, M. Imaging of lipids in cultured mammalian neurons by matrix assisted laser/desorption ionization and secondary ion mass spectrometry. *Surf. Interface Anal.* **2010**, *42* (10−11), 1606−1611.
(55) Silbereis, J. C.; Pochareddy, S.; Zhu, Y.; Li, M.; Sestan, N. The Cellular and Molecular Landscapes of the Developing Human Central Nervous System. *Neuron* **2016**, *89* (2), 248−68.
(56) van Deijk, A. F.; Camargo, N.; Timmerman, J.; Heistek, T.; Brouwers, J. F.; Mogavero, F.; Mansvelder, H. D.; Smit, A. B.; Verheijen, M. H. Astrocyte lipid metabolism is critical for synapse development and function in vivo. *Glia* **2017**, *65* (4), 670−682.
(57) Bieberich, E. Ceramide and sphingosine-1-phosphate signaling in embryonic stem cell differentiation. *Methods Mol. Biol.* **2012**, *874*, 177−92.
(58) Gulbins, A.; Grassme, H.; Hoehn, R.; Wilker, B.; Soddemann, M.; Kohnen, M.; Edwards, M. J.; Kornhuber, J.; Gulbins, E. Regulation of Neuronal Stem Cell Proliferation in the Hippocampus by Endothelial Ceramide. *Cell. Physiol. Biochem.* **2016**, *39* (2), 790−801.
(59) Comi, T. J.; Neumann, E. K.; Do, T. D.; Sweedler, J. V. microMS: A Python Platform for Image-Guided Mass Spectrometry Profiling. *J. Am. Soc. Mass Spectrom.* **2017**, *28* (9), 1919−1928.

https://doi.org/10.1021/jacsau.1c00393
JACS Au 2021, 1, 2261−2270